Floating Catenary Riser System Concept for Brownfield Application

Achoyamen Michael Ogbeifun*[a], Selda Oterkus[a], Julia Race[a], Harit Naik[b], Dakshina Moorthy[c], Subrata Bhowmik[b], Julie Ingram[c].

[a]Department of Naval Architecture, Ocean and Marine Engineering, University of Strathclyde, 100 Montrose Street, Glasgow, G4 0LZ, UK; [b]McDermott International, 40 Eastbourne Terrace, Paddington, London, W2 6LG, UK; [c]McDermott International, 757 N. Eldridge Parkway, Houston, TX 77079, USA.

**corresponding author*; e-mail: achoyamen.ogbeifun@strath.ac.uk, phone: +44 7414 517 860

ABSTRACT

The expansion of a deepwater brownfield may become necessary to increase the production of hydrocarbons. Such expansion often requires the installation of additional risers to the existing floating production platform. However, the seabed footprint of the existing facilities may be congested with existing subsea pipelines and structures. Tying back of risers such as steel catenary riser (SCR) to the floating platform becomes challenging. Floating catenary riser (FCR) is a novel riser solution with floating bends or 'waves' close to the seabed. The FCR is engineered to extend its touch down point (TDP) far beyond the nominal TDP of the SCR and away from the congested seabed footprint. The riser sections before the nominal SCR TDP is configured to float by installing buoyancy modules. The multiple wave buoyant sections also provide the FCR with the capability to decouple its touch down zone (TDZ) from the floating platform motion. This can result in a significant reduction in the stress and fatigue damage around the riser TDP. Presented in this paper are the FCR configuration development and global responses to vessel offsets, current drag load impact, combined load, and wave fatigue loads, simulated to demonstrate the FCR feasibility.

Keywords: Steel catenary riser, floating catenary riser, touchdown point offset, and seabed clearance.

1. INTRODUCTION

Steel catenary risers (SCRs) are widely favoured for greenfield deepwater oil and gas development [1], in environmental conditions that are relatively mild. This attraction to SCR may be attributed to its simplicity and lower cost of procurement compared with other riser types [2]. Hence, many oil and gas fields were developed in the past, implementing SCRs. The needs often arise to expand the capacity of an existing oil and gas field (brownfield) to accommodate economic requirements. This can be driven by the discovery of additional hydrocarbon resources or the need to expand production from existing reservoirs. In some cases, the plan for such additional development may have been poorly considered during the greenfield development resulting in challenges associated with future SCR tiebacks to the existing production floating platform. Suppose the seabed environment around the existing floating platform is congested with subsea structures or environmentally protected features, the new SCR may be challenging or prohibitive as the seabed section can contact these existing subsea systems. The floating catenary riser (FCR) is a new riser solution with a double wave bend close to the seabed, providing its characteristic long span feature over congested or environmentally protected seabed section. It is not easy to achieve this long seabed span with SCR and steel lazy wave risers (SLWR). The FCR concept is proposed in this paper to solve such SCR tieback challenges, as depicted in Figure 1.

The FCR is created by modifying the SCR configuration by installing buoyancy modules on its seabed section. The installed buoyancy system produces multiple wave bends (two-wave bends in this paper). The modification is performed while ensuring that the wave bends are close to the seabed as permissible by the design requirements. The elevation from the seabed of the highest points on the wave bends is the hog elevation (y_{hog}), while the elevation from the seabed of the lowest points in the wave bends is the sag elevations (y_{sag}). The arc height, Δh, is the difference between the y_{hog} and y_{sag} i.e. $(\Delta h = y_{hog} - y_{sag})$.

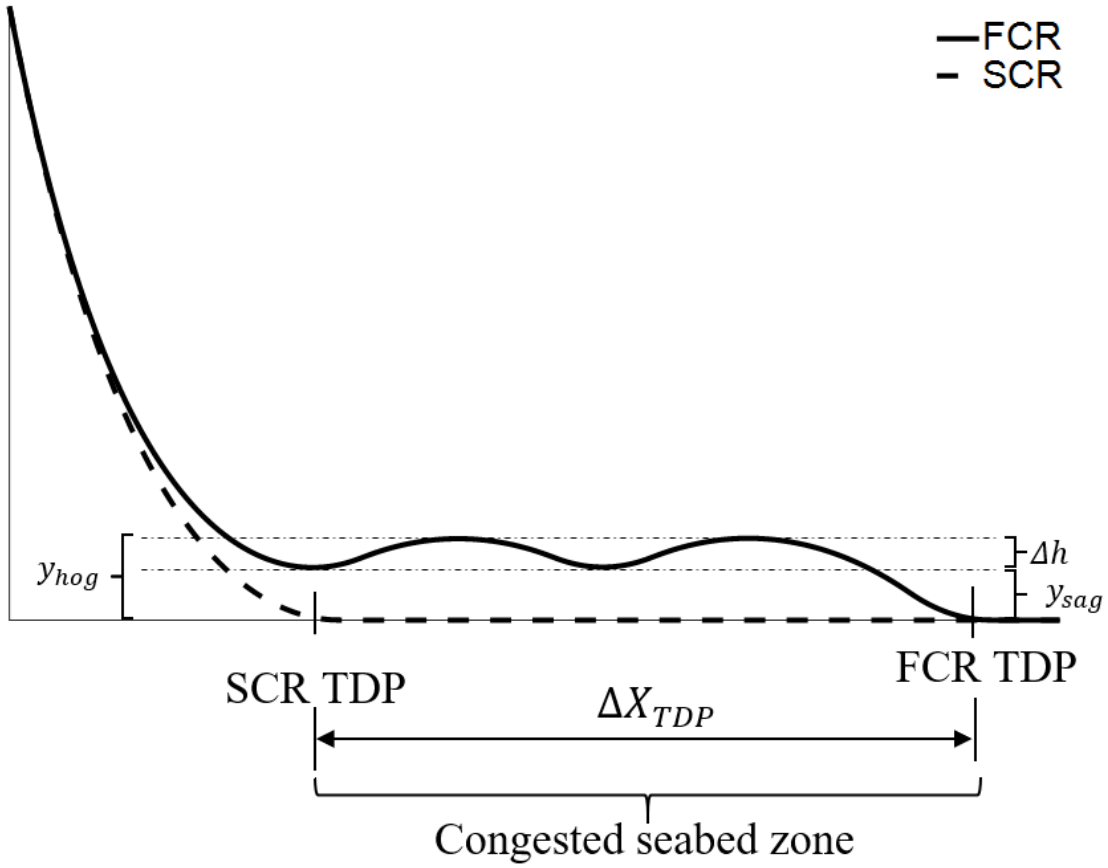

Figure 1. Floating catenary and steel catenary riser configuration

The FCR can be engineered, through the variation of its configuration parameters, to extend its touch down point (TDP) far beyond the SCR nominal TDP and away from the congested section of the seabed within the field. This relative distance between the static FCR TDP and the static SCR TDP is denoted in Figure 1 as ΔX_{TDP} and calculated using equation (1)

$$\Delta X_{TDP} = TDP_{FCR} - TDP_{SCR} \quad (1)$$

The multiple wave buoyant sections also provide the FCR with the capability to decouple its touch down zone (TDZ) from the floating platform motion, a feature typical of steel lazy wave riser (SLWR). This can result in reduced stress and fatigue damage around the touchdown zone (TDZ) when compared with SCR [3]. The configuration development and response of the FCR under different loading conditions is investigated in this paper.

2. FLOATING CATENARY CONFIGURATION

2.1. Initial configuration calculation.

The FCR concept presented in Figure 1 is a specific type of the double wave riser configuration shown in Figure 2, where the arc heights of the two bends are equal, i.e. Δh ($\Delta h_1 = \Delta h_2$), and the sag elevations are equal, i.e. y_{sag} ($y_{sag1} = y_{sag2}$).

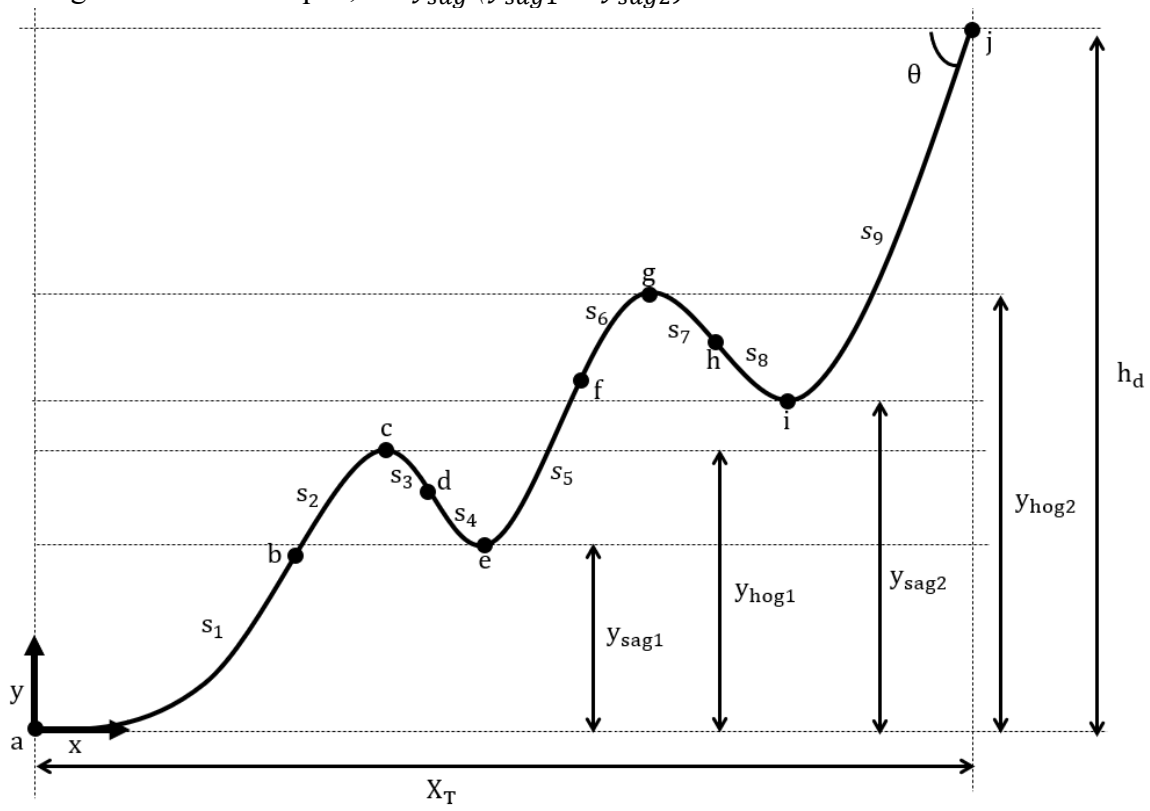

Figure 2. A generic two-wave bend configuration.

One approach to developing the initial configuration of the double wave riser for finite element (FE) models is by decomposing the riser profile into nine (9) basic catenaries, each having its own local origin, as shown in Figure 3. Each of the sub catenaries is calculated referencing their local coordinate systems. They can all be assembled to form the global riser configuration with the global origin at the TDP (point a). The length of the first and second smeared buoyancy sections are $sb_1 = s_2 + s_3$ and $s_{b2} = s_6 + s_7$, where the total buoyant section length is $S_b = s_{b1} + s_{b2}$. Given the configuration height (h_d), the hang-off angle with the horizontal (θ), the sag elevations (y_{sag1} and y_{sag2}) and the hog elevations (y_{hog1} and y_{hog2}), equation (2) to equation (11) were developed for each of the sub catenaries. The horizontal tension component (H) along the profile is constant to ensure continuity of line curvatures across the boundaries of the sub-catenaries. Where x_i, y_i and s_i are the horizontal dimensions, vertical dimensions, and arc lengths of each sub catenaries for $i = 1, 2, \dots, 9$; w is the submerged weight of the bare riser pipe; and w_{b1} and w_{b2} are the submerged weights of the two buoyancy sections. Equation(12) is the assembling equation of all sub catenaries solutions. These sub catenary equations are developed on the cable assumption that the line axial stiffness is infinite and the bending stiffness is negligible. However, they provide high accuracy in the global configuration compared with the resulting finite element model configuration, which includes the bending and axial stiffness effect.

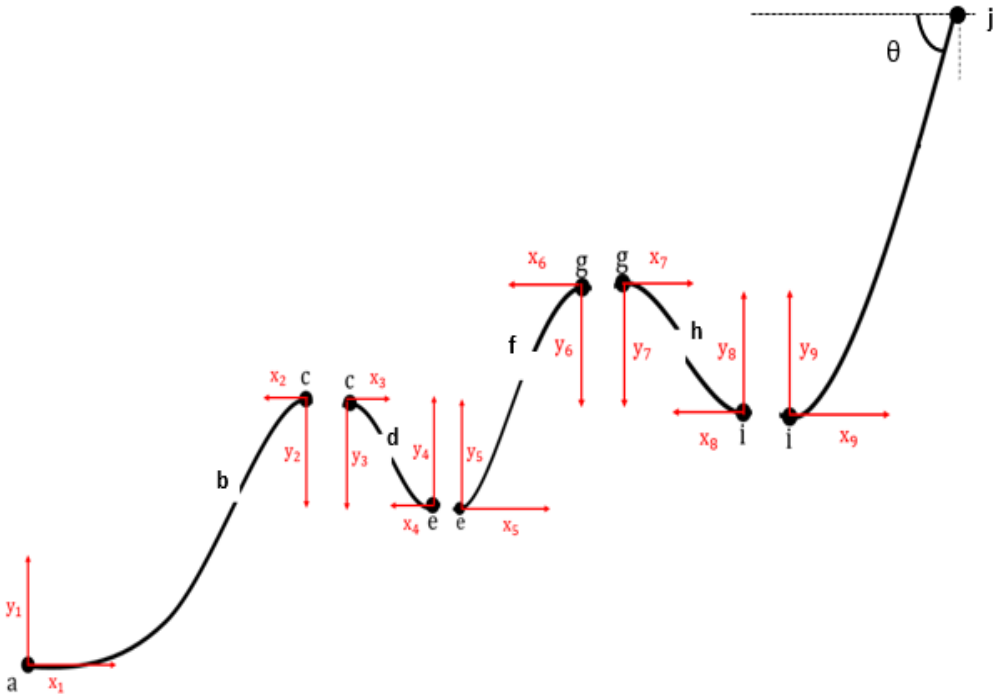

Figure 3. Component catenaries of the two wave configurations.

$$y_9 = h_T - y_{sag2} \tag{2}$$

$$H = H_9 = \frac{wy_9}{(tan\,\theta)^2}(1 + sec\,\theta) \tag{3}$$

$$\begin{cases} x_9 = \dfrac{H}{w} cosh^{-1}\left(\dfrac{wy_9}{H} + 1\right) \\ s_9 = \dfrac{H}{w} sinh\left(\dfrac{wx_9}{H}\right) \end{cases} \tag{4}$$

$$\begin{cases} y_8 = \dfrac{w_{b2}}{(w + w_{b2})}(y_{hog2} - y_{sag2}) \\ x_8 = \dfrac{H}{w} cosh^{-1}\left(\dfrac{wy_8}{H} + 1\right) \\ s_8 = \dfrac{H}{w} sinh\left(\dfrac{wx_8}{H}\right) \end{cases} \tag{5}$$

$$\begin{cases} y_7 = \dfrac{w}{w_{b2}} y_8 \\ x_7 = \dfrac{H}{w_{b2}} cosh^{-1}\left(\dfrac{w_{b2}y_7}{H} + 1\right) \\ s_7 = \dfrac{H}{w_{b2}} sinh\left(\dfrac{wx_7}{H}\right) \end{cases} \tag{6}$$

$$\begin{cases} y_6 = \dfrac{w}{(w+w_{b2})} y_{hog2} \\ x_6 = \dfrac{H}{w_{b2}} cosh^{-1}\left(\dfrac{w_{b2} y_6}{H} + 1\right) \\ s_6 = \dfrac{H}{w_{b2}} sinh\left(\dfrac{w_{b2} x_6}{H}\right) \end{cases} \quad (7)$$

$$\begin{cases} y_5 = \dfrac{w_{b2}}{(w+w_{b2})} y_{hog2} \\ x_5 = \dfrac{H}{w} cosh^{-1}\left(\dfrac{w y_5}{H} + 1\right) \\ s_4 = \dfrac{H}{w} sinh\left(\dfrac{w x_5}{H}\right) \end{cases} \quad (8)$$

$$\begin{cases} y_4 = \dfrac{w_{b1}}{w+w_{b1}} \left(y_{hog1} - y_{sag1}\right) \\ x_4 = \dfrac{H}{w} cosh^{-1}\left(\dfrac{w y_4}{H} + 1\right) \\ s_5 = \dfrac{H}{w} sinh\left(\dfrac{w x_4}{H}\right) \end{cases} \quad (9)$$

$$\begin{cases} y_3 = \dfrac{w}{w+w_{b1}} \left(y_{hog1} - y_{sag1}\right) \\ x_3 = \dfrac{H}{w_{b1}} cosh^{-1}\left(\dfrac{w_{b1} y_3}{H} + 1\right) \\ s_3 = \dfrac{H}{w_{b1}} sinh\left(\dfrac{w_{b1} x_3}{H}\right) \end{cases} \quad (10)$$

$$\begin{cases} y_1 = \dfrac{w_{b1}}{w+w_{b1}} y_{hog1} \\ x_1 = \dfrac{H}{w} cosh^{-1}\left(\dfrac{w y_1}{H} + 1\right) \\ s_1 = \dfrac{H}{w} sinh\left(\dfrac{w x_1}{H}\right) \end{cases} \quad (11)$$

$$X_T = \sum_{i=1}^{9} x_i \, ; h_d = \sum_{i=1}^{9} y_i \; ; S_T = \sum_{i=1}^{9} s_i \quad (12)$$

With the general double wave bend configuration equations, the FCR can then be calculated by setting $y_{sag1} = y_{sag2} = y_{sag}$ and $\Delta h_1 = \Delta h_2 = \Delta h$.

For flexible modelling and analysis, the discrete buoyancy sections are modelled as equivalent smeared (continuous) buoyancy sections with an equivalent thickness (t_b) and outer diameter (D_b), where $2t_b = D_b - D_o$ and D_o is the bare pipe outer diameter. The required buoyancy capacity of the smeared buoyant sections to achieve a given configuration profile can then be determined from t_b or D_b, s_{b1}, s_{b2} and buoyancy material density, ρ_b. What this can imply is that to achieve the required buoyancy capacity, with a given value of ρ_b and different values

of t_b, there will be different corresponding lengths and distributions of the buoyant sections (s_{b1} and s_{b2}). The different buoyant section length will result in different configurations of the FCR. A convenient way to control the geometry of the smeared buoyancy section is the use of the apparent mass ratio (AMR), which is presented in the next section.

2.2. Apparent mass ratio

In this paper, the apparent mass ratio (AMR) of the FCR buoyant sections is taken to be the ratio of the apparent or submerged weight of the buoyant section, w_b, to the apparent or submerged weight of the bare pipe section, w

$$AMR = \frac{w_b}{w} = \frac{w_p + w_c + w_m - B_b}{w_p + w_c - B_p} \tag{13}$$

Where w_p, w_c, w_m, B_b and B_p are respectively the unit weight of bare pipe, unit weight of riser content, unit weight of buoyancy material, unit buoyancy force provided by the buoyant section and unit buoyancy force provided by the bare pipe section. Equation (13) can be expanded and re-casted as equation (14), which provides a relationship between the AMR, the buoyancy material density (ρ_b) and the smeared buoyancy material thickness (t_b). The positive real roots of equation (14) gives the required, t_b for a given AMR and ρ_b. Note that D_i and D_o are respectively the inner and outer diameters of the bare pipe section, and ρ_s, ρ_c and ρ_w are respectively the pipe material, content and seawater densities.

$$At_b^2 + Bt_b + C = 0 \tag{14}$$

Where:

$$A = 4(\rho_b - \rho_w),$$

$$B = 4D_o(\rho_b - \rho_w)$$

$$C = (1 - AMR)\,(\rho_s D_o^2 - \rho_s D_i^2 + \rho_c D_i^2 - \rho_w D_o^2)$$

Hence, for a given $AMR = AMR_1 = AMR_2$, the calculated $t_b = t_{b1} = t_{b2}$ is used to determine $w_b = w_{b1} = w_{b2}$, which are then substituted in the FCR configuration expressions, alongside the configuration variables ($y_{sag}, \Delta h,$ and θ), to obtain the length and distribution of the smeared buoyancy section s_{b1} and s_{b2}.

3. ANALYSIS DATA AND METHODOLOGY

The risers investigated in this study are of 12-inch X70 grade pipes. They are hosted by a generic floating production, storage, and offloading unit at azimuths of 90deg to the vessel heading. The minimum required pipe wall thickness are calculated using DNV-OS-F201 burst and collapse resistance criteria [4]. Table 1 presents the riser data. A generic response amplitude operator (RAOs) for the floating production unit is implemented. Details of the default nonlinear hysteretic riser soil interaction model applied for the analyses can be found in [5]. The two current profiles investigated for the riser systems are presented in Figure 4. The direction of the current is perpendicular to the riser plane to impose the highest lateral drift effect on the risers. The two irregular beam wave loads simulated for the combined load and fatigue analysis are presented in Table 2. The peakedness parameter, γ, is calculated based on [6]. The drag coefficients presented in Table 1 are chosen with reference to the smooth pipe outer diameter. For practical purposes, this value ranges between 0.7 and 1.0 [7], and a value

of 0.7 is selected for the bare pipe section in this study. However, due to the increased diameter of the smeared buoyancy system over the bare pipe section, a conservative drag coefficient of 1.2 is applied for the buoyancy section. The storm wave load selected for the study is typical with Brazil (Campos Basin) 100years return period sea state condition [8]. One of the dominating fatigue sea state condition obtained from fatigue wave scatter is applied for the fatigue analysis, with a probability of occurrence taken as 1. The selected current profile-2 is a 10years return period current with a surface velocity of 1.6m/s [8]. This decreases to 0.1m/s close to the seabed. The constant current profile-1 is theoretical and is only applied to investigate the FCR behaviour under constant current drag load acting on it throughout the water column.

Table 1. Riser data.

Riser data	Values
Pipe size (D_o)	12inch
Internal Design pressure	10ksi
Pipe thickness	27.5mm
Hang off angle with the vertical (90 – θ)	12°
Content density	600kg/m^3
Buoyancy material density (ρ_b)	500kg/m^3
Water depth (h_T)	1500m
Drag coefficient for the bare pipe section	0.7
Drag coefficient for the smeared buoyant section	1.2
Sag elevation (y_{sag})	Vary
Arc height (Δh)	Vary
Apparent mass ratio (AMR)	Vary

Table 2. Combined and fatigue wave load data.

Analyses	Wave type	Data	Values
Storm	Irregular wave	H_s(m)	8
		T_p(sec)	13
		γ	1.6
Fatigue	Irregular wave	H_s(m)	4.5
		T_p(sec)	9.5
		γ	1.8

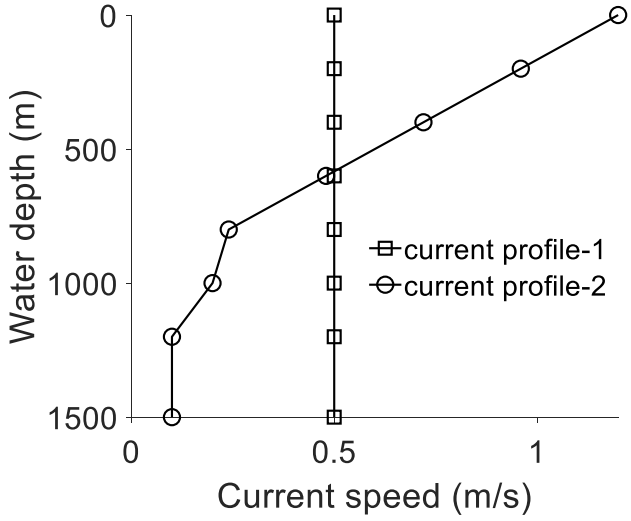

Figure 4. Current load profile for analysis.

The initial configurations for the risers are developed for the FE models using the catenary expressions presented earlier and simulated for the static vessel offset condition, vessel-current load conditions, vessel-current-wave load conditions, and fatigue wave load condition. The numerical simulations of the models are conducted using the OrcaFlex software package. The model pre-processing and post-processing are carried out using MATLAB programs integrated with the OrcaFlex programming interface (OrcFxAPI [9]). The program is used to generate the initial riser configuration for the OrcaFlex models using equation (2) to equation (14). The riser stress utilisations are calculated using the DNV-OS-F201 combined load resistance factor design [4]. The fatigue damage is computed using the rain flow counting technique [10], implementing the S-N D curve for seawater [11].

4. ANALYSIS, RESULTS AND DISCUSSIONS

4.1. Controlling the FCR buoyant section geometry with AMR

The AMR can serve as a single parameter used to vary the geometry (length, thickness, and diameter) of the smeared buoyancy section. To briefly demonstrate the variation of s_{b1}, s_{b2}, S_b and t_b with AMR, an example of FCR with y_{sag} =100m and Δh = 70m is presented in Figure 5. It could be observed that increasing (or decreasing negative) values of AMR provide smaller t_b and a corresponding longer smeared buoyancy section to achieve a given buoyancy capacity. It can also be observed from Figure 5 that the buoyancy section 1, $s_{b1} = s_2 + s_3$ is longer than the buoyancy section 2, $s_{b2} = s_6 + s_7$ for a given AMR. This is expected since the length of the section of the FCR that is lifted by s_{b1} is longer than that lifted by s_{b2}. Hence, the higher required buoyancy capacity of s_{b1} than s_{b2} (both having equal t_b from equal AMR) is compensated by the increased length of the buoyancy section of s_{b1}.

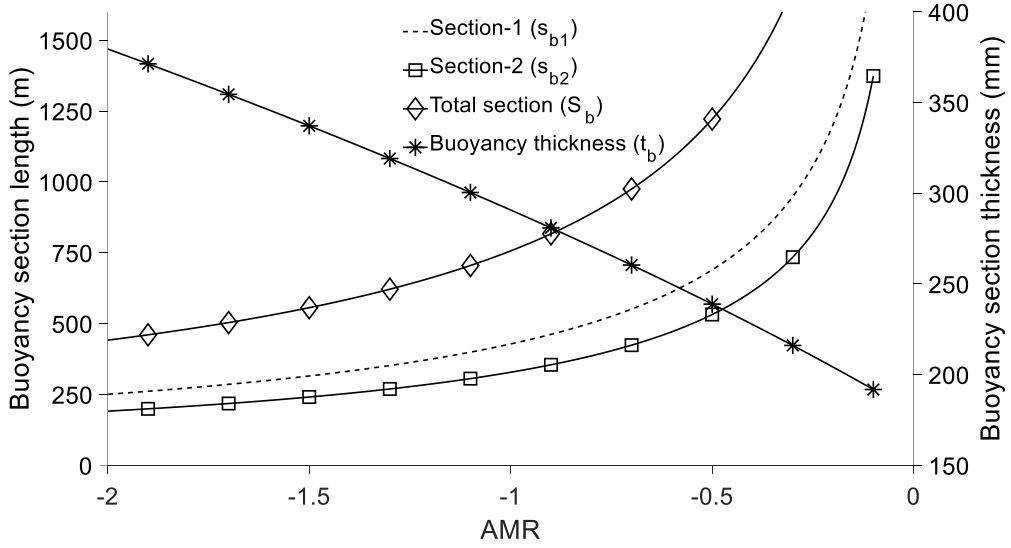

Figure 5. Influence of AMR on buoyancy section geometry.

In this sub-section, we demonstrate the influence of $y_{sag}, \Delta h,$ and θ on the FCR configurations and how these affect the desired ΔX_{TDP}. Six pairs of y_{sag} and Δh , which are {(70m, 10m), (70m, 50m), (70m, 70m), (100m, 10m), (100m, 50m), (100m, 70m)} are simulated for varying values of AMR from -0.15 to -2.00. The considered water depth is 1500m, and the FCRs hang off angle with the vertical (90 - θ) is 12deg. For the same water depth and hang-off angle, a

base SCR configuration is calculated and its TDP relative with the FCR TDPs, ΔX_{TDP}, are computed using equation (1). The resulting configuration curves are presented in Figure 6 (a). For all six combinations of y_{sag} and Δh, the ΔX_{TDP} increases with increasing (or decreasing negativity) AMR. It could be observed from the curves that in terms of a given AMR, it is easier to achieve a desired ΔX_{TDP} for configurations having higher Δh. In fact, increasing the y_{sag} for a given AMR, will have little contribution to the enhancement of ΔX_{TDP}. For example, comparing the configuration corresponding with $(y_{sag}, \Delta h)$ = (70m, 10m), and (100m, 10m), the resulting ΔX_{TDP} are close match. However, for configuration corresponding to $(y_{sag}, \Delta h)$ = (70m, 10m), and (70m, 50m), the ΔX_{TDP} can be increased by more than 500m for a given AMR. Hence, Δh is seen to be a significant influencer of the magnitude of the span that can be achieved for the FCRs for a given AMR. Although in this study, a fixed value of hang off angle (12deg) with the vertical is considered, it may be obvious that ΔX_{TDP} can be increased with increasing hang off angle.

From Figure 6 (a), there are an infinite number of FCR configurations that can be derived from the curves, i.e., from different combinations of the FCR configuration variables - $y_{sag}, \Delta h$ and AMR. However, the key idea behind the FCR concept development is to provide the desired span over the congested section of the seabed. If, for example, ΔX_{TDP} = 1.2km (1200m) is desired, a horizontal line drawn through this point on the ordinate axis intersects the curves at six points, giving six FCR configurations from Figure 6(a). The global configurations of these six FCRs and the base SCR configurations have been presented in Figure 6 (b). A common X_{TDP} and ΔX_{TDP} can be observed for the FCR configurations. However, the configurations are different since unique combinations of the FCR variables resulted in them. Additional configuration details such as the length of the smeared buoyancy sections (s_{b1} and s_{b2}), The overall riser hanging section length (S_T) (see equation (12)), the thickness of the smeared buoyancy material (t_b)(see equation (14), the displacement per unit length of s_{b1} and s_{b2} sections (∇_b) and the overall displacement of s_{b1} and s_{b2} sections ($\nabla_{b_T} = \nabla_b(s_{b1} + s_{b2})$) are presented in Table 3. Note that the outer diameter of the smeared buoyancy section, D_b is $D_o + 2t_b$, where D_o is the outer diameter of the bare pipe. The total displacement of the buoyant sections is seen to be higher for higher Δh values since higher buoyancy capacity is required for higher uplift of the riser hog elevation (y_{hog}). As will be seen shortly, the stress and fatigue response of the FCRs decreases with increasing compliance of the FCR. The compliancy of the FCR is their ability to accommodate stress and fatigue responses, and this requires increased Δh and, consequently, increased ∇_{b_T}.

Recall from Figure 5 that t_b decreases with increasing AMR, resulting in shorter lengths (S_b) of the buoyancy section to provide a given buoyancy capacity, as seen in Table 3. The converse is the case for decreasing values of the AMR. The total hanging length, S_T, of the FCR is jointly affected by the y_{sag}, AMR, Δh and θ for a fixed water depth h. It is interesting to note that the SCR length from the hang off to the common TDP of the FCRs is not significantly different from those of the FCRs (see S_T values in Table 3). This may be attributed to the SCR taking a longer path in its seabed approach compare with the FCRs, although long paths are also seen for the FCRs caused by their wave bend paths. One of the optimisation objectives of the FCR system should be to ensure a minimum difference in S_T of the SCR and the optimum FCR. This is outside the scope of this paper. The lateral deflection, seabed clearance, stress and fatigue damage responses of the six unique FCR configurations in Figure 6 (b) will now be investigated under extreme vessel offsets, current loads, combined loads, as well as fatigue wave load in the remaining parts of this paper, to demonstrate the FCR global feasibility.

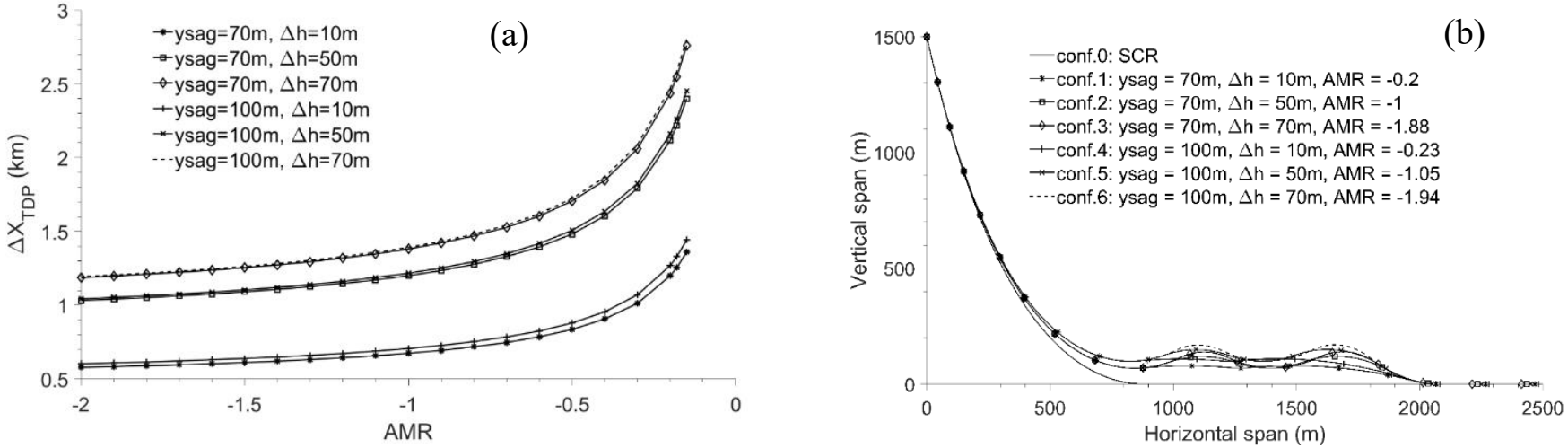

Figure 6. (a) – Influence of FCR configuration variables on ΔX_{TDP}, (b) – Selected six configurations that provide ΔX_{TDP} =1.2km.

Table 3. Selected FCRs configuration details.

Conf	Riser type	y_{sag} [m]	Δh [m]	AMR [-]	s_{b1} [m]	s_{b2} [m]	S_b [m]	t_b [m]	D_b [m]	∇_b [te/m]	∇_{b_T} [te]	S_T^* [m]	X_{TDP}^{**} [m]	ΔX_{TDP}^{**} [m]
0	SCR	-	-	-	-	-	-	-	-	-	-	3053.00	885.44	0
1	FCR	70	10	-0.20	681.72	354.11	1035.83	0.20	0.70	0.40	414.22	3014.25	2085.44	1200.00
2	FCR	70	50	-1.00	359.81	278.52	638.32	0.29	0.88	0.63	402.30	3046.26	2085.31	1199.87
3	FCR	70	70	-1.88	249.03	202.94	451.97	0.37	1.04	0.88	397.18	3071.86	2085.70	1200.26
4	FCR	100	10	-0.23	703.39	322.77	1026.16	0.21	0.72	0.42	433.98	2996.61	2082.00	1196.56
5	FCR	100	50	-1.05	370.76	265.84	636.60	0.30	0.90	0.66	419.55	3038.01	2086.69	1201.25
6	FCR	100	70	-1.94	256.81	195.83	452.64	0.37	1.04	0.88	397.77	3063.50	2085.17	1199.73

Note:

* The values of S_T reported for the FCRs are the hanging lengths, i.e., from the hang off to their common TDP. However, the values reported for the SCR (Conf-0) is the length of the SCR from its hang off to the common TDP of the FCRs. The hanging length of the SCR is 1852.85m.

** The X_{TDP} and ΔX_{TDP} are reported from FE models (OrcaFlex), which are slightly varied from the analytical X_{TDP} and ΔX_{TDP} = 1200m (1.2km). The maximum absolute percentage error between the analytical and the numerical values is 0.29%. This demonstrates the suitability of the developed analytical models applied for defining initial FCR configurations for the FE models.

4.2. Extreme vessel offsets analysis

One of the most critical design variables to be observed for the extreme vessel offsets of the FCRs is the minimum seabed clearance of the wave bends sections depicted in Figure 7. The minimum seabed clearance is taken to be the minimum vertical distance between the bottom section of the FCR wave bends and the seabed. The feasibility of the FCR depends on its configuration performance in extreme offsets conditions, especially the near offset condition, which can result in a significant reduction in the nominal seabed clearance, hence defeating the FCR application need.

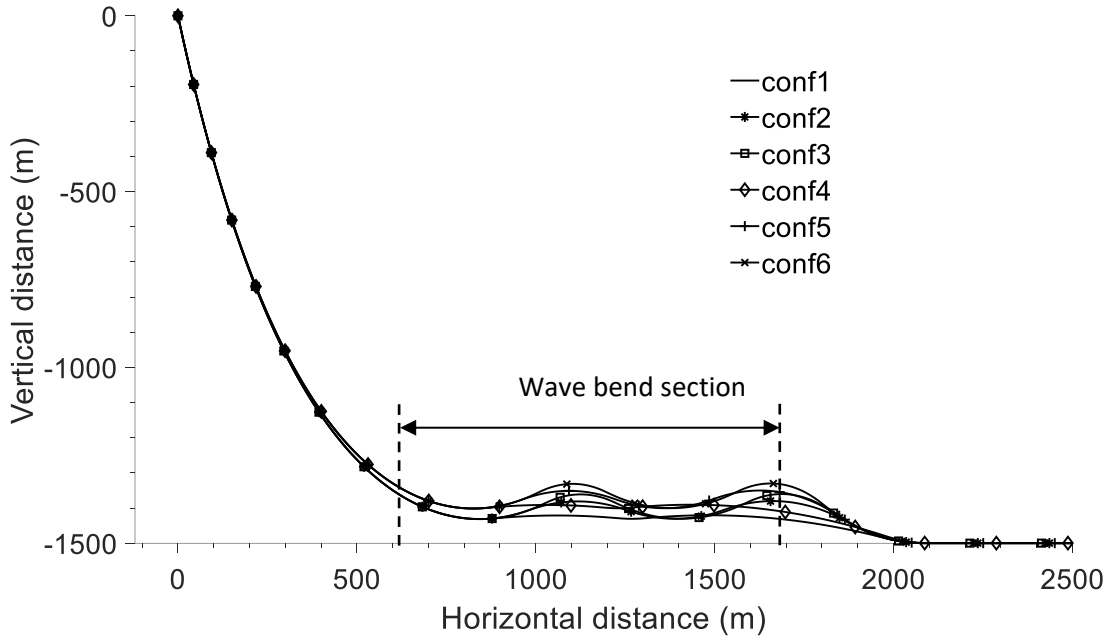

Figure 7. Wave bend section for which critical seabed clearance should be checked in extreme vessel far and near offsets.

A vessel offsets of 8% of the water depth ($h = 1500$m) in the near direction (towards the risers' seabed anchor) and the far direction (away from the risers' seabed anchor) are imposed on the FCRs. The resulting global configurations for the near and far offsets are respectively presented in Figure 8 (a) and (b). The criticality of the seabed clearance can be seen for the extreme near configurations in Figure 8 (a) around the wave bend on the vessel side, caused by the global compression of the FCRs. The far configuration resulted in the increase of the nominal seabed clearance, as seen in Figure 8 (b), caused by the stretching of the global riser configuration. A comparison of the seabed clearance for the nominal, the near and far vessel offset configurations are presented in Figure 8 (c). Figure 8 (d) shows the percentage difference of the FCRs seabed clearances in their offsets positions relative to the nominal seabed clearance. For all the six FCR configurations considered in this analysis, the nominal clearance can be reduced by more than 40% compared with the nominal configuration. The clearance reduction can be as high as 85% for conf-1, which has the smallest y_{sag} and Δh as seen in Figure 8 (d).

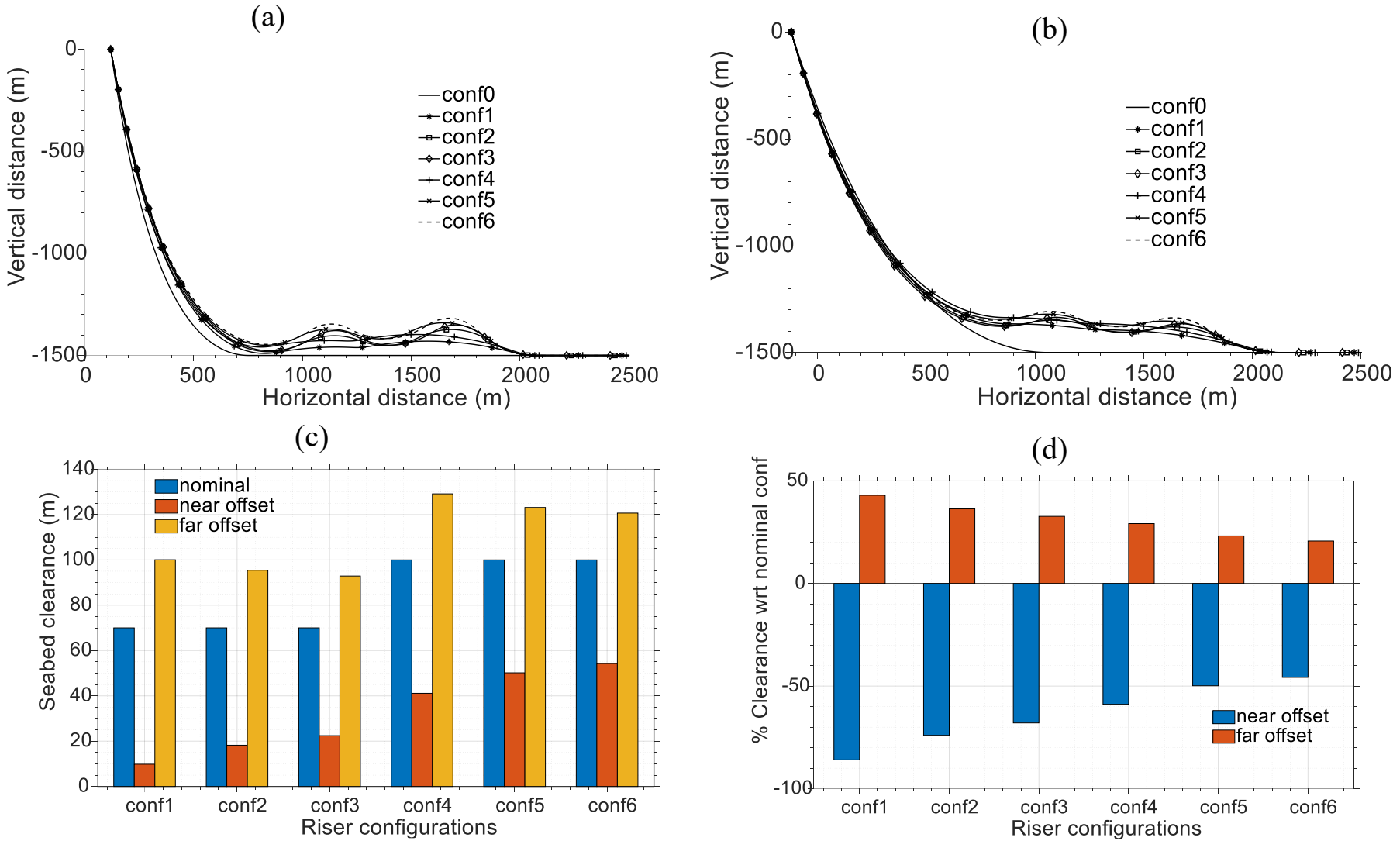

Figure 8. (a) risers' configurations in the vessel's extreme near offset condition, (b) risers' configurations in the vessel's extreme far offset condition, (c) minimum seabed clearance of the FCRs in the vessel's extreme nominal, near and far offset conditions, (d) minimum seabed clearance relative to the nominal seabed clearance expressed in percentages.

Considering the FCR configurations of equal y_{sag}, increasing Δh will result in little improvement of the resulting minimum clearance for the FCRs in their near configuration. For example, for conf-2 and conf-3 with equal y_{sag} of 70m, but with respective Δh of 10m and 50m, the seabed clearance for conf-3 in the near configuration is around 10% higher than conf-2. The reverse is the case for the far configuration where increasing values of Δh for fixed y_{sag} performs less in terms of the minimum seabed clearance, although these clearances are still higher than those of the nominal configuration. Significant performance in the seabed clearance can be achieved in the FCR near configurations, for higher y_{sag} values. For example, comparing conf-1 and conf-4, with equal $\Delta h = 10m$ and different y_{sag} of 70m and 100m respectively, conf-4 can perform more than conf-1 up to 30%. These seabed clearance behaviours of the FCRs indicate that clearance performance in the extreme near configuration can be jointly improved by increasing y_{sag} and Δh. However, these increases will imply an increase in the required buoyancy capacity. Hence, there is a need to strike a balance between the FCR performance in terms of the minimum seabed clearance in the extreme near offset condition and the cost associated with the buoyancy capacity required for the configuration.

4.3. Current loading analysis

Current loads impose statical drift effects on the risers, causing them to deflect globally. The risers' lateral deflections are of more importance since excessive deflection in this direction can result in functional failure of the riser systems as well as interference with other neighbouring systems. The magnitude of the lateral deflection is dependent on the current profile velocities, the drag coefficients of the riser section, the projected drag area of the riser to the current flow direction, and the global stiffness of the riser, which depends on effective tension distribution. The projected hydrodynamic areas of the risers are presented in Figure 9, for the bare pipe, the buoyancy, and the sum of both the bare pipe and the buoyancy sections. It could be seen that the projected areas of the smeared buoyancy sections for all FCR configurations, except conf-1 and conf-4, are larger than the projected area of the bare pipe sections. Also, the drag coefficient of the smeared buoyancy section can be higher than that of the bare pipe section. In this work, the drag coefficients for the smeared buoyant section and the bare pipe section are taken to be 1.2 and 0.7, respectively (see Table 1).

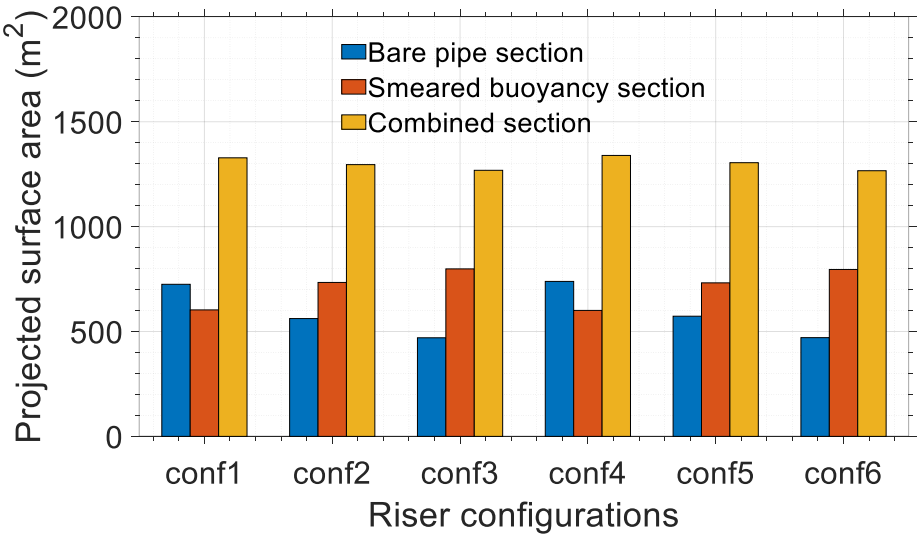

Figure 9. Projected surface areas of FCRs to current cross flow

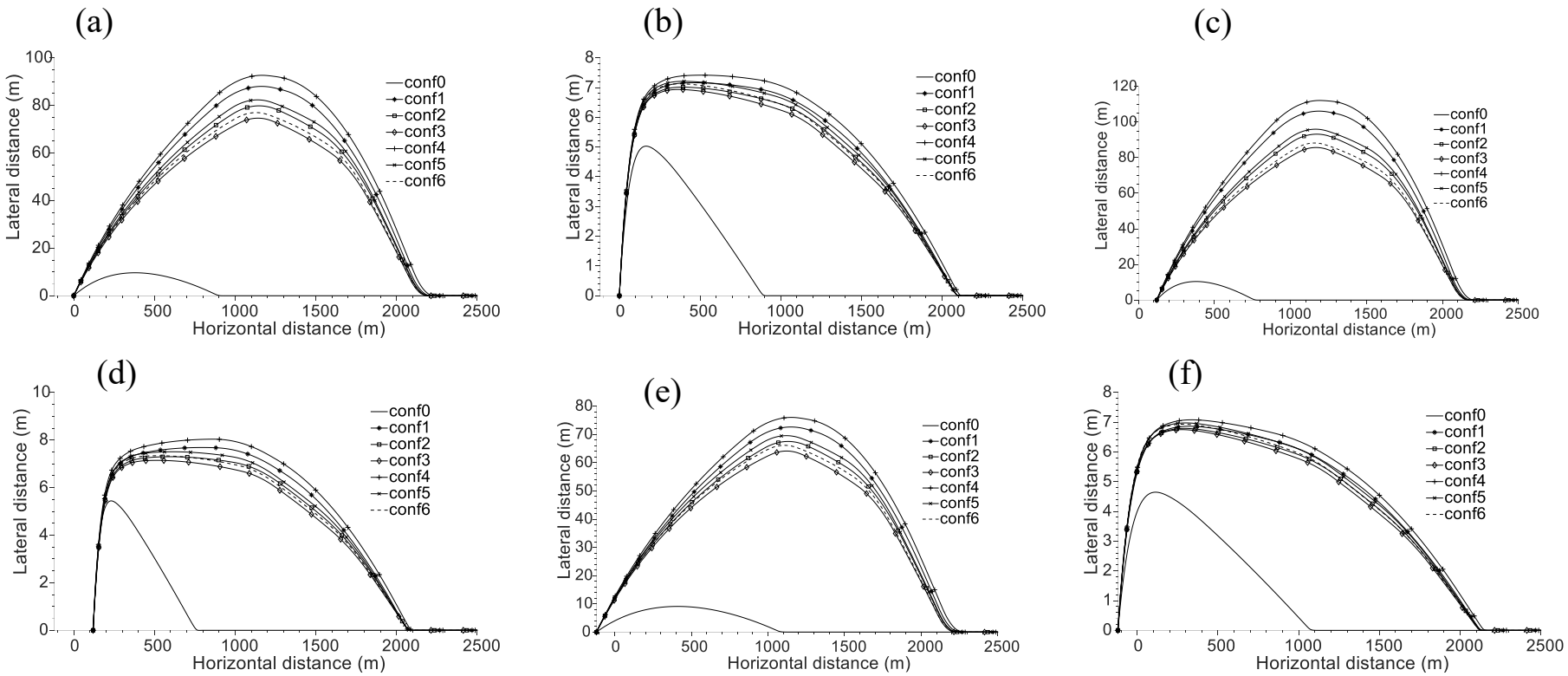

Figure 10. Minimum seabed clearance for FCRs under (a) nominal offset condition plus current profile-1, (b) nominal offset condition plus current profile-2, (c) near offset condition plus current profile-1, (d) near offset condition plus current profile-2, (e) far offset condition plus current profile-1, (f) near offset condition plus current profile-2

The two current profiles (profile-1 and profile-2) are imposed on the risers in the nominal, near and far vessel offset conditions. The static lateral deflection responses of the risers under current loads and vessel offsets are presented in Figure 10. The current load intensity of current profile-1, being more intensive than current profile-2, resulted in the highest lateral deflections for the same vessel offset conditions. This is observed when Figure 10 (a), (c) and (e) are respectively compared side by side with Figure 10 (b), (d) and (f). The near vessel offset is the most critical offset condition for which the riser being in global compression (increased slackness) has reduced global stiffness to the current load. The highest lateral deflections of the risers under current profile-1, in the near offset condition, is observed to be about 120m. On the other hand, the maximum deflection under current profile-2 in the near vessel offset condition is about 8m. However, it should be noted that the constant velocity profile-1 is unrealistic but can be useful for investigating a novel system like this. For each of the vessel offset positions and current profiles combination, the FCRs experienced different magnitudes of lateral deflections. The lateral deflection increases for conf-3, conf-6, conf-2, conf-5, conf-1, and conf-4, in that order. This order corresponds with the magnitude of the combined projected area presented in Figure 9, indicating the influence the hydrodynamic area of the riser can have on their global deflection under current load. The riser seabed clearances under current drift conditions are expected to be less critical compared with the cases where only vessel offsets are applied. This is because the lateral deflection of the risers will reduce the vertical clearance component from the seabed.

The general conclusion from the lateral deflection behaviour of the FCRs is that they may be functionally limited in an environment where there exist intensive current profiles close to the seabed. This is because the largest projected area of the riser to current flow and largest current drag force exists on FCR sections close to the seabed. However, the FCR should be feasible in an environment with a minimum current profile close to the seabed, such as current profile-2 investigated in this paper. Riser interference may be less of a problem since little difference in the riser plane (angular deviation on the horizontal plane) will result in a large gap of the FCR wave bends close to the seabed, considering deepwater. Also, the current load impact on neighbouring FCRs will result in a drift of the risers in the same direction, keeping their nominal distance almost unchanged, except in cases where the risers undergo large amplitude motions under VIV. This can be designed out following practical design recommendations [12].

4.4. Seabed clearance under extreme and damaged vessel condition

In addition to the extreme offsets, excess vessel heel caused by vessel damage condition may also impact the seabed clearance of the FCRs wave bends. The vessel damaged condition is modelled by imposing static vessel heel of 8deg in the direction of riser azimuth on the extreme vessel offsets, storm wave load and the current profile-2. Both the FCRs' seabed clearances under extreme and damaged conditions are compared with those of the static nominal FCRs configurations to observe their influence on the FCRs.

The FCRs' minimum seabed clearances under extreme condition (storm wave load, vessel offsets and current profile-2) are presented in Figure 11. The minimum seabed clearances under vessel damaged conditions (storm wave load, vessel offsets, current profile-2 and vessel heel of 8deg) are presented in Figure 12. For the FCRs considered in this paper, the nominal and far vessel offset conditions for both extreme and damage scenarios provide no threat to the seabed clearance of the FCRs. However, the near vessel offset condition can significantly negatively impact the FCRs' seabed clearances under these conditions.

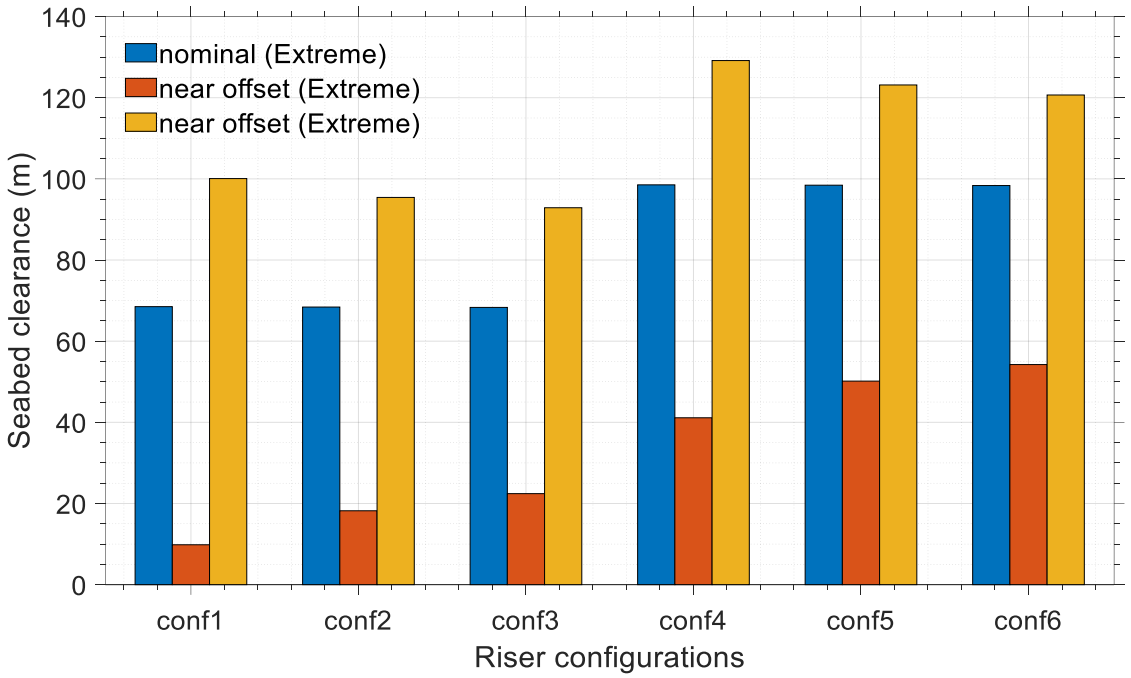

Figure 11. Minimum seabed clearances of FCRs during combined load extreme conditions (storm wave, current profile-2, and vessel offsets)

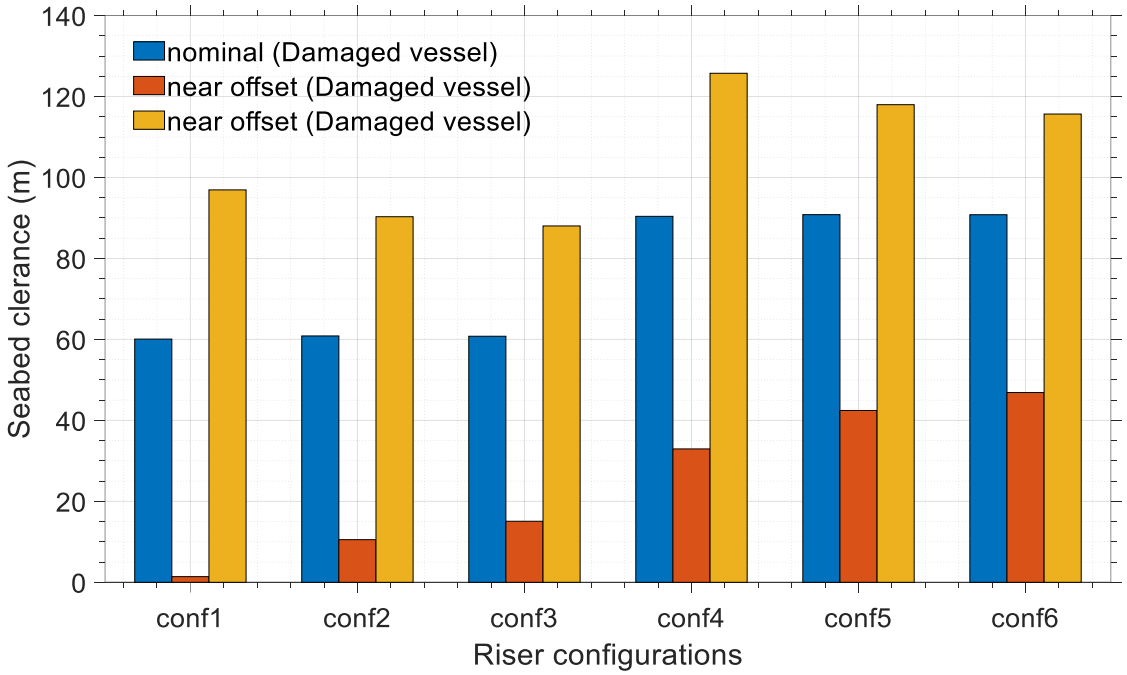

Figure 12. Minimum seabed clearances of FCRs during combined load and vessel damaged conditions (storm wave, current profile-2, vessel offsets and vessel damaged condition)

The minimum seabed clearances for the near vessel offsets for both the extreme and the damaged conditions are compared with seabed clearances of the static nominal FCR configuration in Figure 13. It could be observed from Figure 13 that the seabed clearance requirement can be violated when the vessel is damaged and in its near offset configurations. Hence, the damaged condition at the preliminary stage of FCR configuration selection must be put into consideration to select suitable static FCR profiles that give the required seabed clearance for all design scenarios. Similar behaviour of seabed clearance reduction is observed for the extreme response, as seen in Figure 13. However, the damaged conditions, as expected,

is more critical and should be the driver or determining factor that limits the minimum seabed clearance during the FCR design.

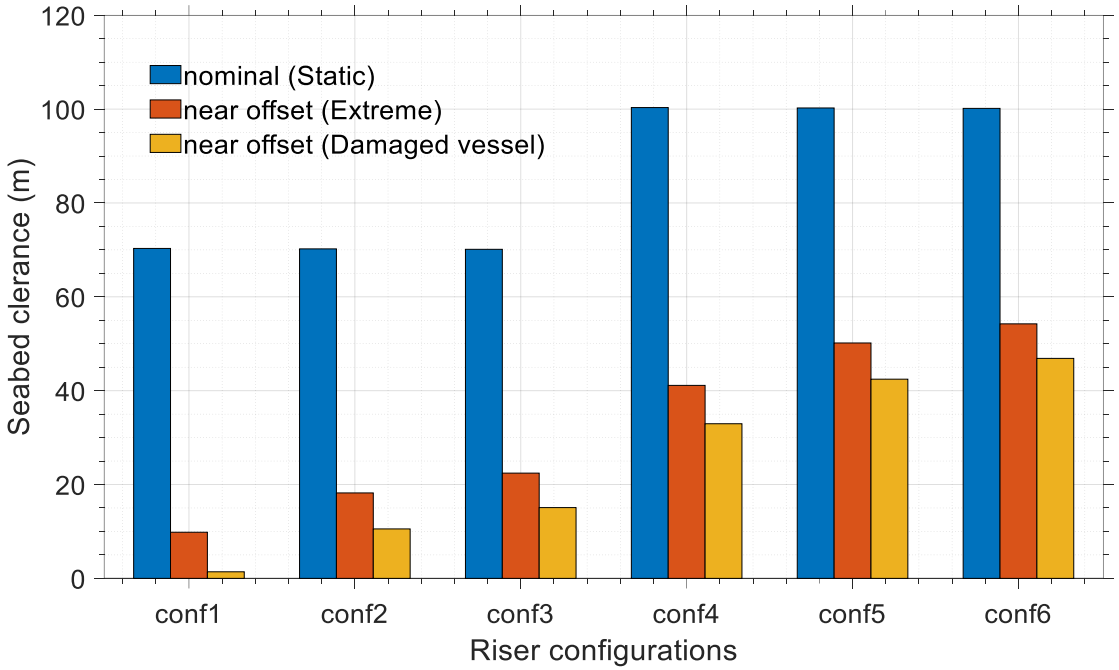

Figure 13. Minimum seabed clearance of FCRs in static nominal vessel position compared with the seabed clearance of FCRs in near vessel offset for extreme and vessel damaged conditions.

4.5. Dynamic stress utilisation

The storm wave load in Table 2, each of the three-vessel offset conditions, and the current profile-2 are jointly imposed on the risers. The wave loads and vessel offsets are applied in the riser azimuth direction, while the current load is applied perpendicular to the riser plane. As a result, there will be time-varying bending moments and resulting stresses, as well as tension generated in the risers. The resulting stresses in the risers are expressed as the stress utilisation computed based on the DNV-OS-F201 combined load criteria [4]. The stress utilisation for the risers in the nominal, near and far offset conditions are presented in Figure 14 (a), (b) and (c), respectively. The highest stress utilisation is observed close to the dynamic TDP of the SCR (conf-0), where a sharp peak of the stress is observed. The reduction in the FCRs' stress utilisation (compared with SCR) is attributed to the decoupling capability of the wave bends of the risers from the vessel motions. This results in the reduced and more regular distribution of the bending stresses along the wave bends and the FCRs' TDZs. A general inspection of the plotted stress utilisation distribution in the FCR wave bend section shows that conf-2 and conf-5 (with $AMR \approx$ -1) have the least stress response in the three vessel offsets condition. It could also be observed that conf-1 and conf-4 (with the shorter Δh) possess higher stress utilisation peaks around the wave bend section and the TDZ as seen in Figure 14 (a), (b), (c) and (d). This indicates that the decoupling of the FCR TDZ by the wave bends is dependent on Δh. This stress response behaviour dependency on Δh is similar to that of the SLWR [13]. However, as mentioned earlier, higher Δh will require higher buoyancy capacity and an increased associated riser cost. A balance between the stress response and buoyancy cost need to be considered during the optimisation of such a system. Generally, as observed from the results, the peak stress of FCRs appear to be less sensitive to the different vessel offset conditions under dynamic loading, when compared with those of the SCR.

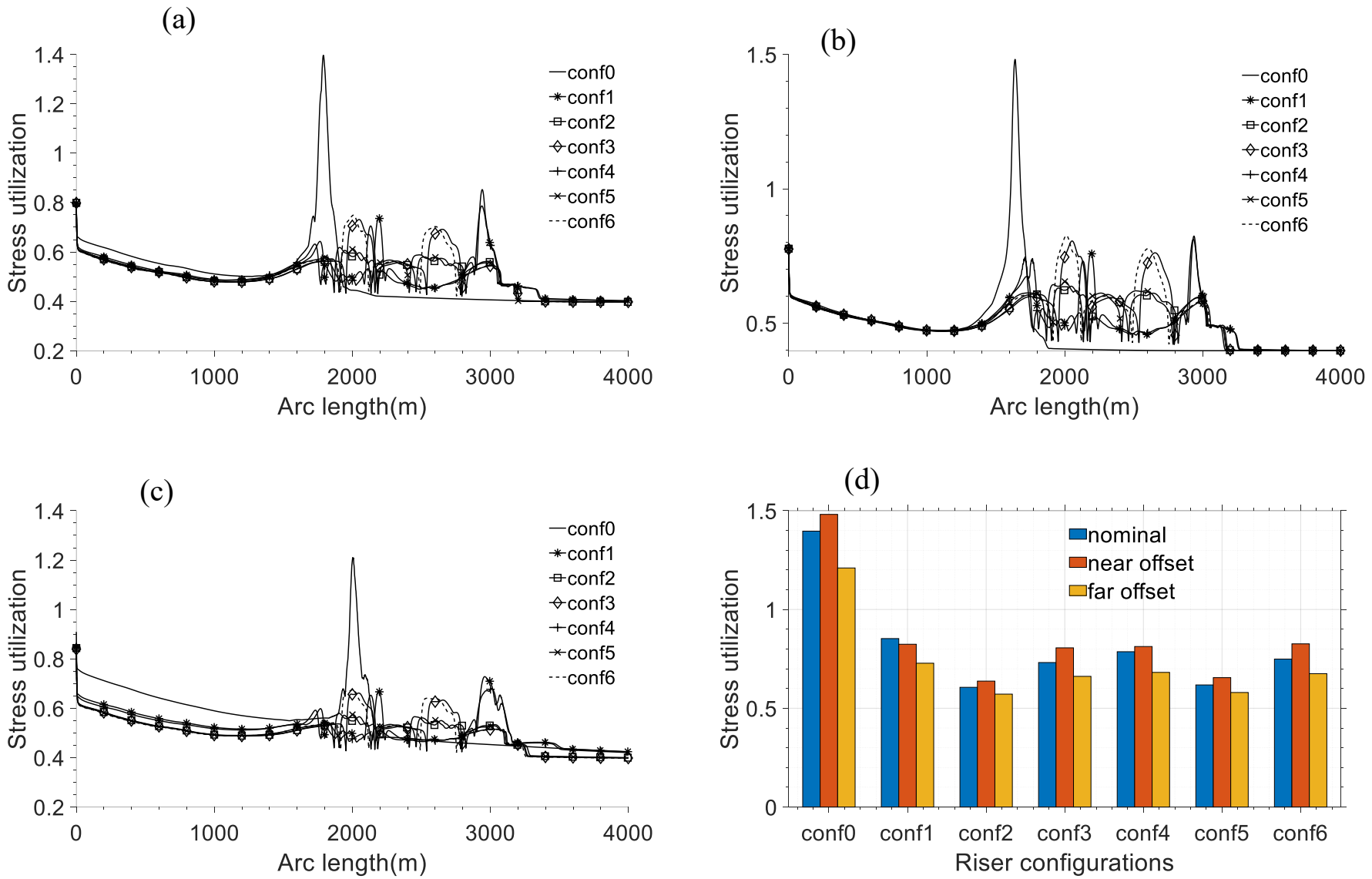

Figure 14. (a) Risers stress utilisation (storm wave load, nominal offset, and current profile-2), (b) Risers stress utilisation (storm wave load, near offset, and current profile-2), (c) Risers stress utilisation (storm wave load, far offset, and current profile-2), (d) Bar chart plot comparing stress utilisation for the three combined load scenarios.

4.6. Dynamic maximum and minimum tension

A characteristic response of the SCR is its high-top dynamic tension, which is higher for larger hang-off angle and deeper water column. The highest top tension is expected to be seen for risers in their far configurations since the longer section of the riser will be hanging for this condition. Therefore, only the dynamic tensions in the risers far offsets are presented in Figure 15 (a). However, a comparison of the maximum dynamic top tensions for the riser in the three offsets conditions are presented in Figure 15 (c). One of the benefits of the SLWR is the reduced top tension due to the upward pull of a section of the riser. Increased submerged weight reduction is achievable when the buoyancy section is installed on the higher sections of the riser from the seabed. However, for the FCR, the buoyancy modules are installed at the possible lower parts of the riser close to the seabed. Hence, the weight reduction may not be as significant as that of the SLWR. It is worth noting that the FCRs can still achieve an appreciable level of reduction in the dynamic top tensions. As seen in Figure 15 (a) and (c), more than 300kN reduction is observed for all FCRs compared with the SCR.

Buckling is one of the challenges of SCR around its TDZ. The global buckling tendencies of the SCR around its TDZ can be characterised by effective negative tension. Since the near offset condition contributes more to the global riser compression at the TDZ than the nominal and far vessel offsets, the near offset configuration is expected to increase the buckling tendencies or cause increased negative tensions in the risers. Therefore, only the minimum effective tensions of the risers in their near offset conditions are presented in Figure 15 (b). However, a comparison of the minimum effective tension for the three-vessel offset conditions is presented in Figure 15 (d). The SCR is seen to be in higher compression under the combined loading conditions. Nevertheless, all FCRs have positive minimum effective tension, although FCR configurations with shorter values of Δh such as conf-1 and conf-4 are seen to be in higher compression around the wave bends than other FCR configurations. This behaviour is also typical with the steel lazy wave riser [13].

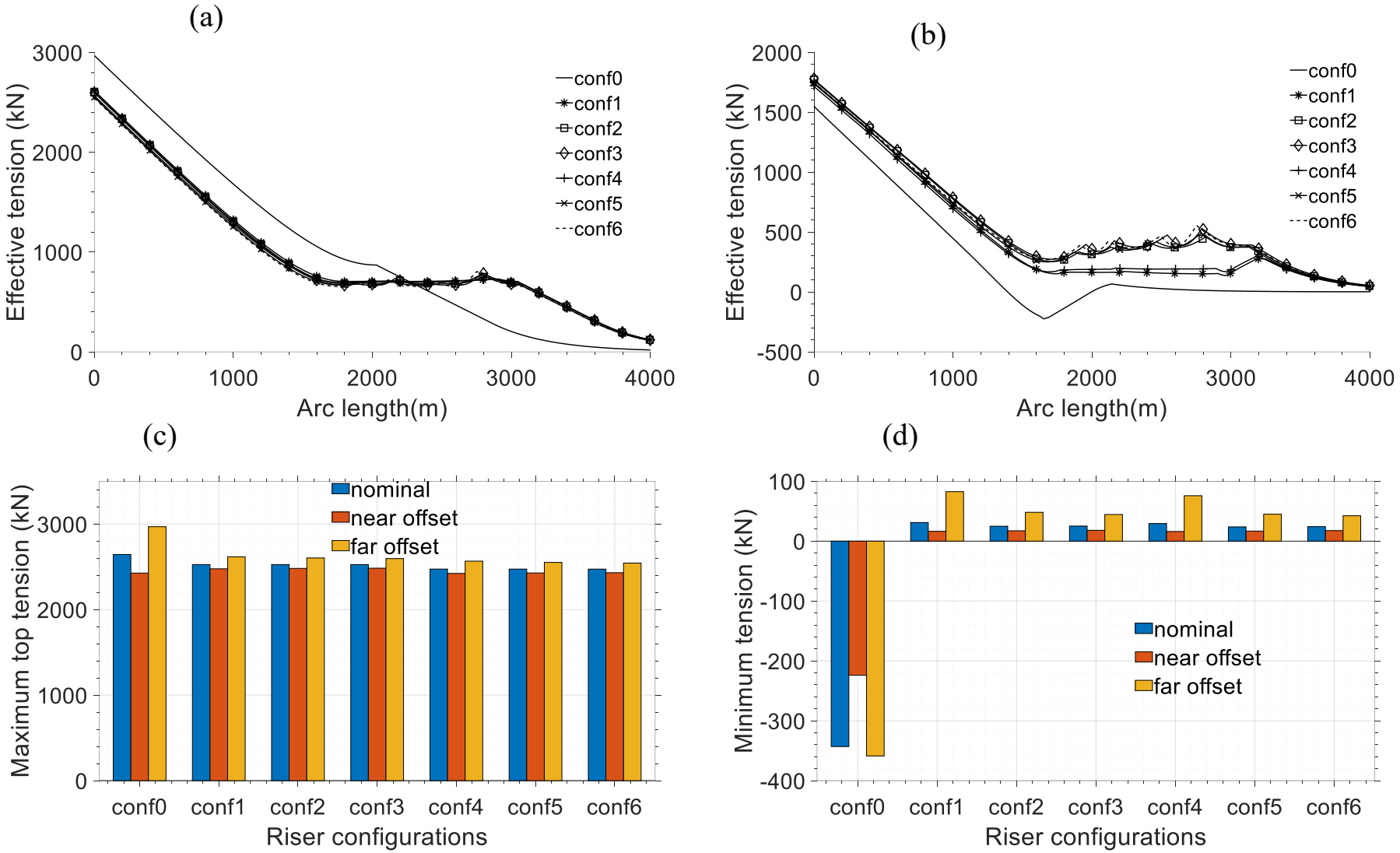

Figure 15. (a) Risers maximum effective tension (storm wave load, far offset, and current profile-2), (b) Risers minimum effective tension (storm wave load, near offset, and current profile-2), (c) Bar chart plot comparing maximum effective tension for the three combined load conditions, (d) Bar chart plot comparing minimum effective tension for the three combined load conditions.

4.7. Fatigue load analysis

The fatigue analyses for the risers are conducted with the risers in their nominal position, with the wave load acting in the riser azimuth direction. No current load was applied for the fatigue analysis. The fatigue damage responses along the risers are plotted on a semi-log scale in Figure 16, the peak fatigue damage responses are plotted on a log scale in the bar chart presented in Figure 17 (a), and the peak fatigue damage of the FCRs normalised by the peak fatigue damage of the SCR (conf-0) are plotted in normal scale in Figure 17 (b). Generally, the fatigue damages are observed from Figure 16 to be highest around the wave bends and the TDZ as expected for all riser configurations. The SCR possesses the most serious fatigue damage compared with all FCRs. However, as shown in Figure 16 and Figure 17 (a), conf-1 and conf-4 have a comparative damage response with that of the SCR (conf-0). This is due to their characteristic shorter Δh, which reduces their compliance to fluctuating bending moment and stresses caused by the vessel response to the fatigue wave load. In fact, as the Δh approaches zero, the FCRs behaves like the SCR in terms of the fatigue damage response. Hence, shorter arc heights (Δh) of the FCR wave bends are not favourable for both stress utilisation and the fatigue damage responses. The conf-2, conf-3, conf-5 and conf-6 with the highest Δh are seen to have good performers in terms of the fatigue damage response. One can also observe from Figure 16 and Figure 17 (a) that the fatigue performance can be improved by increasing y_{sag}. For FCRs with equal Δh, the configuration with higher y_{sag} have better performance (in terms of fatigue damage) than configuration with lower y_{sag}. For example, conf-5 which has higher y_{sag} than conf-2 possess smaller peak fatigue damage than conf-2, although both of them have equal Δh. Higher values of Δh and y_{sag} will therefore improve the fatigue performance of the FCR. However, higher buoyancy capacity and associated cost of the buoyancy modules will be required to achieve higher Δh and y_{sag}. Hence, an optimum FCR configuration should be able to achieve the desired ΔX_{TDP}, maintain the require minimum seabed clearance in the extreme and damaged near offset conditions, and be able to cut down significantly on the stress utilisation and fatigue damage responses, at a minimum cost of the riser and its buoyancy system.

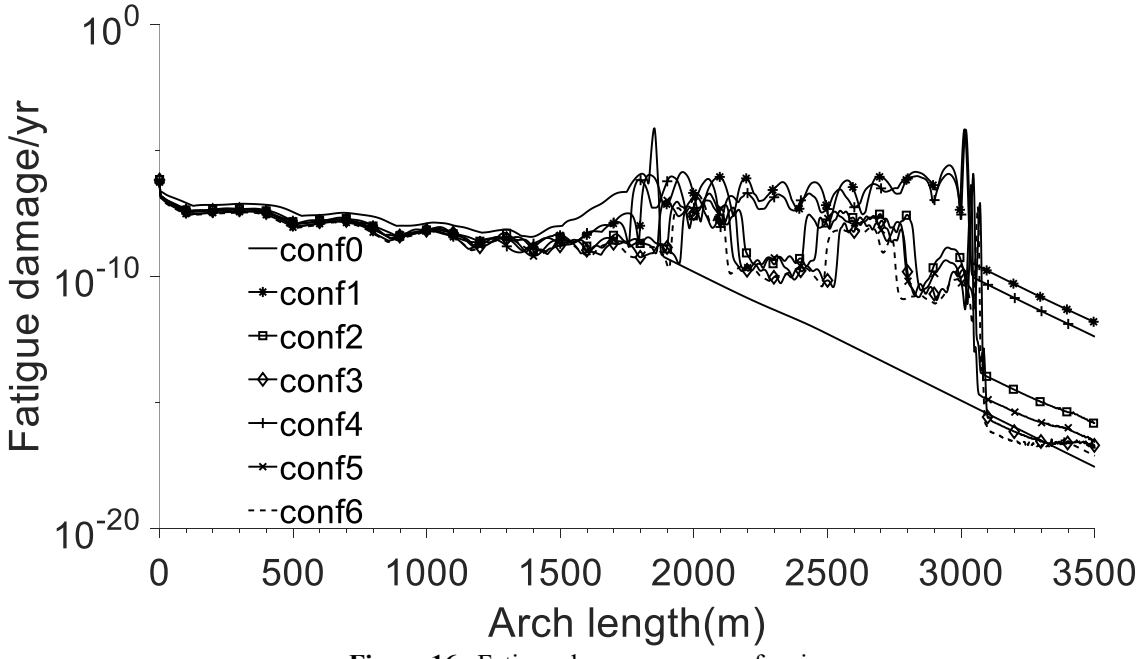

Figure 16. Fatigue damage response for risers

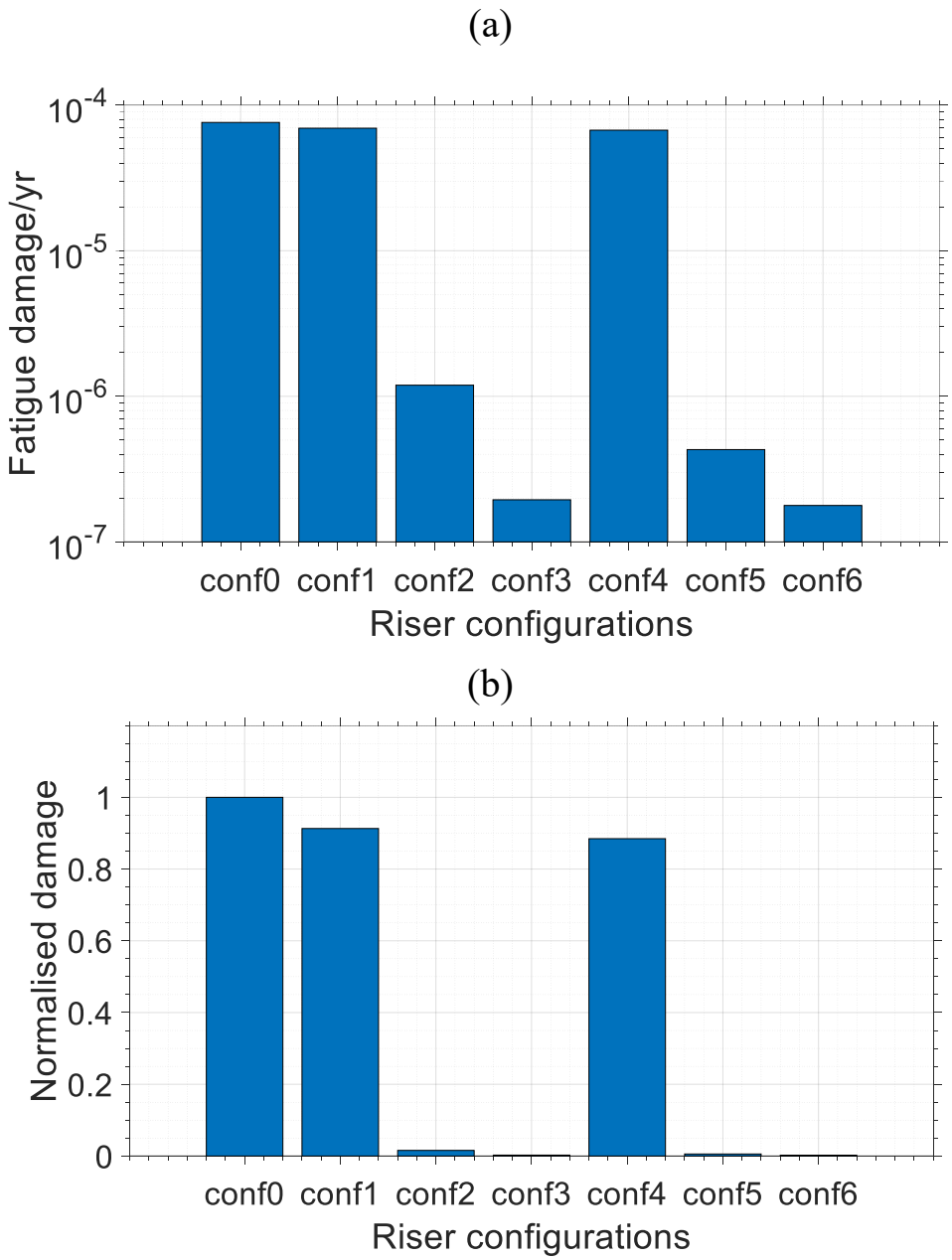

Figure 17. (a) peak fatigue damage response, (b) peak fatigue damage response normalised by SCR peak fatigue

5. CONCLUSION

The development and feasibility investigation of a novel riser, the floating catenary riser (FCR), is presented in this paper. The FCR concept is being developed to address the challenges associated with additional SCR tiebacks during a brownfield expansion. Expanding a brownfield may be necessary when the production capacity of the field is to be ramped up. However, if the potential seabed path of the SCR is congested, the tie back can be impossible. The FCR can provide the opportunity to extend the SCR nominal TDP far beyond the congested seabed zone by an offset (ΔX_{TDP}). The FCR is characterised by two-wave bends of equal sag and arc height elevation, created by the installation of buoyancy modules on the seabed section of the SCR. The buoyant section provides an uplift to the SCR seabed section, ensuring that that desired minimum seabed clearance between the riser and the congested seabed is achieved in all loading conditions. The two-wave buoyant sections also provide the FCR with the

capability to decouple its TDZ from the floating platform motion. This can result in a significant reduction in the stress and fatigue damage around the riser bends and TDZ. To demonstrate the feasibility of the FCR concept, configuration variables, responses under static vessel offsets, responses under combined loading conditions, and fatigue damage responses under fatigue wave loading are investigated in this paper. The following features are observed for the FCR:

- Three configuration variables, the sag or hog elevation (y_{sag} or y_{hog}), the arch height (Δh) and the apparent mass ratio (AMR) are important for the easy control of the FCR configuration or profile. A combination of these three variables can result in an infinite number of configurations. However, an optimum configuration will be required to achieve the design seabed clearance and touch down point extension (ΔX_{TDP})
- Increasing values of AMR result in reduced smeared buoyancy thickness and a longer buoyancy section for a given required buoyancy capacity. An $AMR \approx$ -1 provides an FCR configuration with increased performance in stress utilisation.
- The y_{sag} and Δh controls the elevation of the FCR wave bends from the seabed. Increased values of the two variables increase the compliancy of the FCR and can help to significantly reduce the fatigue damage response when compare with the conventional SCR. As Δh values approach zero, the FCR fatigue damage can be as serious as those of the conventional SCR.
- The vertical minimum seabed clearance of the FCR above the congested seabed is an important output variable that must be looked out for if the FCR must achieve its purpose. This clearance can become very critical for vessel near offset conditions where the riser is in global compression resulting in a significant reduction in the clearance between the FCR wave bends and the seabed. However, suitable design values of y_{sag} and Δh can help to address this problem.
- Because the buoyancy sections are quite close to the seabed, the reduced top tension provided by the FCR concept compared to those of the SLWR can be moderate. However, when compared with the dynamic top tension of the SCR, the FCR can be said to provide an appreciable reduction in the top tension. The compression in the FCRs, measure by the negativity of the minimum effective tension is seen to be lower for the FCR compare with the SCR under dynamic condition. This indicates improved performance against global buckling when compared with those of the SCR.
- The FCR, because of its longer buoyancy section, can be prone to significant lateral deflection under intensive current loads. This limits the FCR application to regions where the current profile towards the seabed is minimum.

In general, the seabed clearance, the top tension, the compression, the stress, and the fatigue response can be improved by higher values of y_{sag} and Δh. However, the required buoyancy capacity to achieve higher values Δh and y_{sag} can introduce negative cost implication. Hence, an optimum FCR configuration should be able to achieve the desired ΔX_{TDP}, maintain the required minimum seabed clearance in the extreme near offset condition, and be able to cut down significantly on the stress utilisation and fatigue damage responses, at a minimum cost of the riser and its buoyancy system. The choice of an optimum FCR configuration can be derived through an optimisation process, where the objective function will be ΔX_{TDZ}, and the cost associated with the buoyancy sections (S_b) and the total riser hanging length (S_T). The design variable will be the AMR, y_{sag} and Δh. The constraint functions will be the stress utilisation, fatigue damage, deflection under current load and the corresponding minimum seabed clearance. The development of such a methodology is a subject of ongoing research.

During brownfield expansion for increased economic benefits, the cost of the FCR due to the installed buoyancy modules required to achieve the FCR configuration can be high compared with the conventional SCR. However, considering the cost of doing nothing, i.e., no riser installation, due to the constraint posed by the congested seabed, the FCR concept is worth considering.

RECOMMENDATION

For the FCR, the wave bend section under intensive current profile can be a “hot region” for vortex-induced vibration (VIV) fatigue damage. The VIV fatigue damage response needs to be investigated in future work as part of the feasibility study for the FCR. Since this study focuses on the general feasibility response of the FCR, the optimisation of the FCR configuration (optimum combination of AMR, Y_{sag} and Δh) is not covered here. The FCR optimisation analysis is an ongoing work.

ACKNOWLEDGEMENTS

The authors acknowledge the University of Strathclyde and McDermott International for their support. Results in this work were obtained using the ARCHIE-WeST High-Performance Computer (www.archie-west.ac.uk) based at the University of Strathclyde.

REFERENCES

[1] R. Song and P. Stanton, "Advances in Deepwater Steel Catenary Riser Technology State-of-the-Art: Part I—Design," 2007: American Society of Mechanical Engineers, pp. 331-344.

[2] L. M. Quéau, M. Kimiaei, and M. F. Randolph, "Sensitivity studies of SCR fatigue damage in the touchdown zone using an efficient simplified framework for stress range evaluation," *Ocean Engineering,* vol. 96, pp. 295-311, 2015.

[3] B. Yue, D. Walters, W. Yu, K. Raghavan, and H. Thompson, "Lazy wave SCR on turret moored FPSO," in *The Twenty-first International Offshore and Polar Engineering Conference*, 2011: International Society of Offshore and Polar Engineers.

[4] D.-O. Standard, "F201, 2010," *Dynamic Risers. DNV: Norway*.

[5] M. Randolph and P. Quiggin, "Non-linear hysteretic seabed model for catenary pipeline contact," in *ASME 2009 28th International Conference on Ocean, Offshore and Arctic Engineering*, 2009: American Society of Mechanical Engineers, pp. 145-154.

[6] D. N. Veritas, "DNV-RP-C205 Environmental conditions and environmental loads," *Det Norske Veritas: Oslo, Norway,* 2010.

[7] R. Song and P. Stanton, "Advances in Deepwater Steel Catenary Riser Technology State-of-the-Art: Part II—Analysis," in *ASME 2009 28th International Conference on Ocean, Offshore and Arctic Engineering*, 2009: American Society of Mechanical Engineers Digital Collection, pp. 285-296.

[8] G. DNV, "DNVGL-OS-E301 Position Mooring," *DNV GL, Oslo,* 2015.

[9] L. Orcina, "OrcaFlex User Manual: OrcaFlex Version 10.2 c," *Daltongate Ulverston Cumbria, UK,* 2018.

[10] M. Matsuishi and T. Endo, "Fatigue of metals subjected to varying stress," *Japan Society of Mechanical Engineers, Fukuoka, Japan,* vol. 68, no. 2, pp. 37-40, 1968.

[11] D. N. V. As, "DNV RP C203 Fatigue Design of Offshore Steel Structures," ed: Norway, 2010.
[12] D. N. Veritas, "Riser Interference," *DNV Recommended Practice F,* vol. 203, 2009.
[13] A. Felisita, O. T. Gudmestad, D. Karunakaran, and L. O. Martinsen, "Review of steel lazy wave riser concepts for the north Sea," *Journal of Offshore Mechanics and Arctic Engineering,* vol. 139, no. 1, p. 011702, 2017.